APPLICATIONS OF EQUILIBRIUM OF CONFIGURATIONAL FORCES FOR THE MEASUREMENT OF COHESIVE LAWS

Ulf Stigh

School of Enginnering, Mechanics of Materials, University of Skövde, Skövde, Sweden
Email: ulf.stigh@his.se, Web Page: http://www.his.se/MechMat

Keywords: Configurational forces, Experimental method, Adhesive, Kink-band, Composite

Abstract
A methodology to develop experimental methods to measure cohesive laws is introduced. This methodology is based on the property of all configurational forces equilibrium acting on a specimen to be in equilibrium. Two applications are given. The first shows a method to measure the cohesive law for shear representing the mechanical behaviour of an adhesive layer. The second application is a method to measure the cohesive law for the formation of a kink-band in a unidirectional composite. It is concluded that the methodology is critically dependent on the ability to associate a pseudopotential to the inelastic properties of the deforming material where the fracture process takes place. The importance to clearly identify the material that is modelled with the cohesive zone is also stressed.

1. Introduction

The concept of configurational forces was introduced in the theory of elasticity by Eshelby (1951), cf. [1]. It has later been extended to inelasticity, for an overview cf. [2]. It provides almost unexplored possibilities for the development of experimental methods to measure cohesive laws associated with fracture. In the present paper, the concept is introduced and examples of developed test set-ups are given. These comprises methods to measure cohesive laws associated with fracture of adhesives, cf. [3], and kink-band formation due to compressive loading of a unidirectional (UD) composite, cf. [4]. The paper is organized with a brief recapitulation of the theory of configurational forces followed by examples of designed experimental methods to measure cohesive laws.

2. Configurational forces and cohesive zones

We limit ourselves to hyperelasticity with a strain energy density function U. In parts of a test specimen modelled with conventional continuum mechanics, the components of the stress tensor are given by $\sigma_{ij} = \partial U/\partial \varepsilon_{ij}$ where ε_{ij} is the components of the strain tensor. In parts modelled with cohesive zones, the components of the cohesive traction are given by $\Sigma_i = \partial U/\partial \delta_i$ where δ_i is the separation vector. Thus, U depends explicitly on the position. Index notation is used with the lower case subscript indicating the coordinate; summation is to be taken over repeated indexes, and a comma indicates partial differentiation. The function U is allowed to vary in a restricted manner with the coordinates; it can be considered as two separate functions – one for the conventional continuum and another for the cohesive zone. A Cartesian coordinate system is used and the considered test specimens are essentially two-dimensional with x_1 oriented along the cohesive zone and x_3 out of the plane of the specimen.

With the present orientation of the cohesive zone, the x_2 components of the cohesive traction and the separation vectors are denoted σ and w, respectively; the x_1 components are τ and v, respectively. For

Excerpt from ISBN 978-3-00-053387-7

short, they are denoted the peel (σ , w) and shear components (τ , v), respectively. The basic problem can be stated as: Provided data from measurements of an experiment is available, what is the cohesive law $\sigma(w)$ or $\tau(v)$; or in mixed mode loading, what is $\sigma(v,w)$ and $\tau(v,w)$? As shown here, equilibrium of configurational forces is used to design experimental methods to measure these relations.

The configurational force $\mathbf{P}_I$ on an object I in the direction $\mathbf{x}_I$ is defined by

$$\mathbf{P}_I = -\frac{\partial \Pi}{\partial \mathbf{x}_I} \tag{1}$$

where Π is the potential energy of the body. Coordinates are given in a Cartesian frame. Thus, any identifiable object in an elastic field that changes the potential energy if it is moved is, by definition, an *object* in this respect. Readily identifiable objects are boundaries, positions of load application and inhomogeneities in material properties. If all objects have been identified, Eq. (1) shows that the sum of all the configurational forces is zero since an infinitesimal repositioning of all objects in the same direction and by the same amount leaves the body in exactly the same state as its original state. Thus, the total variation of Π is zero and the configurational forces are in *equilibrium*.

Some objects in elasticity are related to unbounded properties of the elastic fields. One such object of special interest here is a force **F**. Kelvin's solution shows that the stress tends to infinity as the point of load application is approached, cf. e.g. [5]. Formally, the potential energy is un-bonded and a straightforward application of Eq. (1) is unfeasible. This difficulty is solved by splitting the fields into two parts, one associated with a force in an infinite body (i.e. Kelvin's solution) and one part associated with the rest so that the displacement field, i.e. $\mathbf{u} = \mathbf{u}^{\mathrm{s}} + \mathbf{u}^{\mathrm{a}}$, where superscript s and u indicate Kelvin's singular solution and the remainder, respectively. An evaluation, [6], of the configurational force P_{F} in the x_1 direction of a force F acting in the x_2 direction yields

$$P_{\mathrm{F}} = F\theta \tag{2}$$

where $\theta \equiv -u^{\mathrm{a}}_{i,j}$. If θ cannot be considered small, θ is replaced with $\sin(\theta)$ in Eq. (2), cf. [7]. More generally, the configurational force on object I in the x_1 direction can be calculated using

$$P_I = \int_{S_I} \left(U n_{\square} - T_i u_{i,\square} \right) \square S \tag{3}$$

where S is *any* closed surface confining *only* object I. It may include other objects provided these do not change the energy of the specimen if they are moved in the x_1 direction, i.e. an object is allowed to reside inside S if its configurational force has components in the x_2- and/or x_3-directions but no component in the x_1-direction. Moreover, **n** and **T** are unit outward normal and outward traction vector on S.

Equation (3) provides the configurational force P_{C} of a cohesive zone. First assume that the cohesive zone has a finite thickness h and imagine S to be a cuboid centred at the start of the cohesive zone. Let the dimension in the x_3-direction, l_3, coincide with the width b of the cohesive zone and l_2 to be minutely larger than h so that the cuboid encapsulates the cohesive zone. Finally, shrink the length in the x_1-direction, l_1, to zero. Since $\mathbf{T} = \mathbf{0}$ at the free edge of the cohesive zone, only the first term remains in Eq. (3). Assuming no variation out of the plane yields after a change of variables

$$P_{\mathrm{C}}(v,w) = b\int_0^w \sigma(v,\tilde{w})\,\mathrm{d}\tilde{w} + b\int_0^v \tau(\tilde{v},w)\,\mathrm{d}\tilde{v} \tag{4}$$

Now, h does not enter Eq. (4) and it is valid also in cases of cohesive zones without thickness. Equations (2) and (4) provides the foundation for the specimen configurations presented here. By designing specimens where the forces act in the x_2-direction, only one cohesive zone is active in the x_1-

Excerpt from ISBN 978-3-00-053387-7

direction, and no other configurational forces contribute, equilibrium of these forces provides P_C and after differentiation, the cohesive laws $\sigma(v,w)$ and $\tau(v,w)$. Examples are provided below.

3. Adhesive joints

A generic specimen with an adhesive layer with thickness h is presented in [8], cf. Fig. 1. By equilibrium, two of the four acting forces can be expressed in the remaining two forces. By setting $F_3 = F_4 = 0$, equilibrium yields $F_1 = F_2$ and a Double *Cantilever Beam Specimen* (CBS) results. By symmetry, this specimen yields a pure peel loading of the adhesive layer. By setting $F_1 = -F_2$ an *End Notched Flexure* (ENF) specimen results. By symmetry, this specimen loads the adhesive layer in pure shear. With F_2 and F_4 as reaction forces from supports, the *Mixed Mode Bending* (MMB) specimen results. Most of these specimens can be designed to provide stable crack growth and a gradual reduction of the acting loads during an experiment, cf. [9].

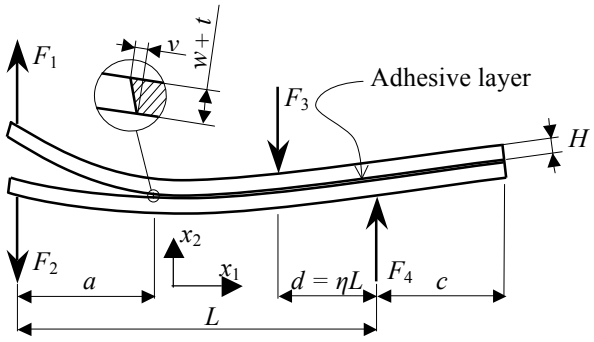

Figure 1. Deformed generic specimen adapted from [8].

With cohesive zone modelling of the start of the adhesive layer, two alternative expressions can be derived for the configurational force on the cohesive layer with thickness h used to represent the adhesive. Equation (4) directly yields P_C provided the cohesive law is known and if we measure w and v (indicated in Fig. 1) during an experiment. If the cohesive law is unknown, as is generally the case, the alternative expression for P_C is derived from Eq. (3) by using S enclosing the complete specimen. Thus, S is the surface of a cuboid. The two surfaces with unit normal in the $\pm x_3$-direction do not contribute to P_C. The first term in the integrand of Eq. (3) is identical zero since the normal of the surfaces do not have any component in the x_1-direction and $n_1 = 0$. Moreover, these surfaces are traction free and the second term in the integrand is also zero. Hence, these surfaces do not contribute to P_C.

The two surfaces with normal in the $\pm x_1$-direction can be designed to give negligible contributions to P_C. No forces act on these surfaces. Thus, the second term in Eq. (3) is zero since the traction is zero. The first term can give contributions if the distance c between the point of load application and the free edge is too small. That is, if considerable stresses occur at the free edge. The contribution is easily predicted using FE-analysis and the geometry in Fig. 1 is exaggerated; smaller overhangs than indicated in the figure can be tolerated.

On the remaining surfaces with normal in the $\pm x_2$-direction, the first term in Eq. (3) does not contribute. However, each of the acting forces gives a contribution to P_C according to Eq. (2). This yields the alternative expression

$$P_C = F_1\theta_1 - F_2\theta_2 - F_3\theta_3 + F_4\theta_4 \tag{5}$$

Excerpt from ISBN 978-3-00-053387-7

Now, by setting the two alternative expressions equal, i.e. Eqs. (4) and (5), the cohesive law can be derived by proper differentiation of the resulting expression provided v, w, F_1, F_2, F_3, and F_4 are measured continuously during an experiment. Note that two of the four forces are directly given from the remaining two by equilibrium.

An example is provided in [10] where the cohesive law in shear is measured with an ENF-specimen for the epoxy adhesive DOW-Betamate XW-1044-3 with h = 0.2 mm. In this case, F_3 is denoted F and F_1=-F_2 and F_4 are reaction forces. After utilizing this and setting Eqs. (4) and (5) equal, we arrive at

$$\tau = \frac{1}{b}\frac{\partial}{\partial v}\left[\eta F\theta_1 - F\theta_3 \square\left(1-\eta\right)F\theta_4\right] \tag{5}$$

where η is defined in Fig. 1 and where $\theta_2 = \theta_1$ by symmetry. Figure 2a shows the measured configurational force per unit width $J \equiv P_C/b$ vs. the shear deformation v. The curve shows a first maximum at about 2.1 kN/m. This value corresponds to the shear stress equal to zero at a critical shear deformation of about v_c = 0.14 mm, cf. Fig. 2b. Thus, at this stage a crack has formed and the fracture energy equals 2.1 kN/m. The maximum stress is about 22 MPa. The details of the experiments are given in [10].

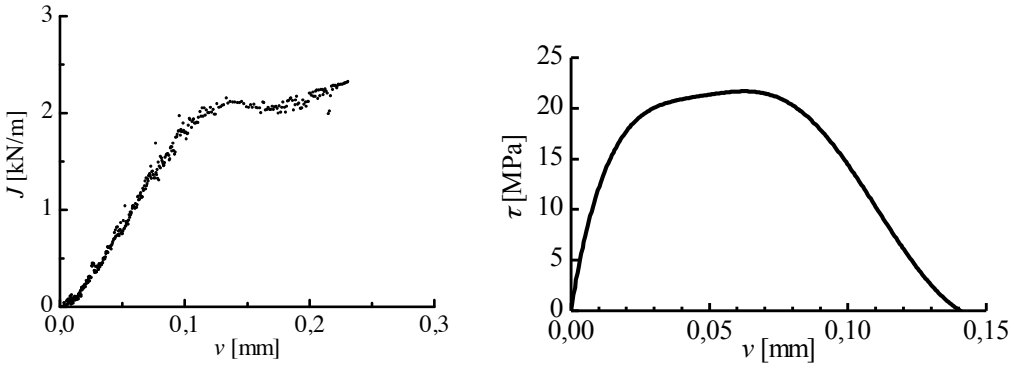

Figure 2. a) Measured configurational force per unit with vs. v; b) Derived cohesive law, [10].

4. Compressive fracture of composite

Compressive loading in the fibre direction of high-performance composite materials is often limited by the formation of a kink-band. This consists of a thin zone of collapsed fibres that extends through the thickness of a ply and has a considerable length in the plane of the composite. Thus, the geometry of the kink-band suggests that it can be modelled by a cohesive zone. A method to measure the cohesive law associated with the formation of a kink-band in a UD-composites is developed based on the equilibrium of configurational forces, cf. [4]. Figure 3 illustrates the main features of the specimen.

Excerpt from ISBN 978-3-00-053387-7

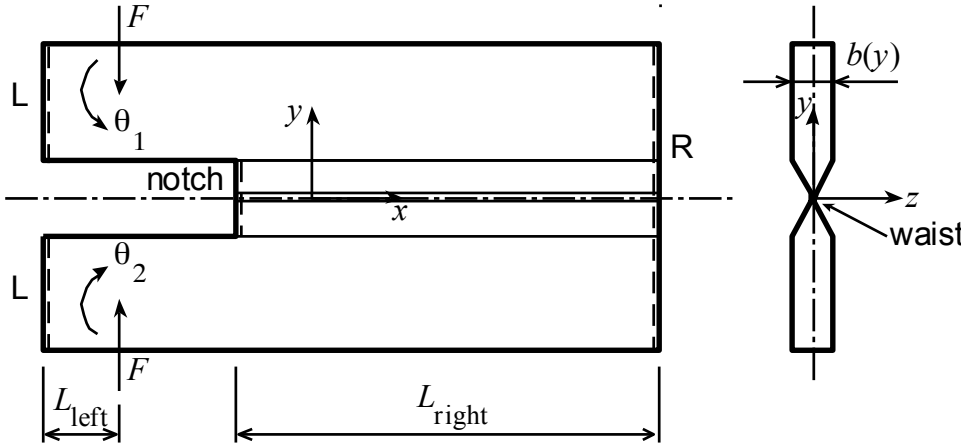

Figure 3. Main features of the specimen developed in [4].

The material is HTS carbon fibre in a RTM6 resin. One of the main difficulties to measure the cohesive law corresponding to kink-band formation in a UD-composite is to transmit the load F into the intended position of the kink-band without initiating in-elastic response of the material in other positions than at the kink-band. To this end, cross-laminates are used in the upper and lower parts of the specimen, i.e. the parts with the constant thicknesses, cf. Fig 3b. By ply-dropping and machining, a waist is formed at the symmetry line $y = 0$. The wedge-shaped parts of the specimen constitute objects with configurational forces in the y-direction. However, no horizontal configurational forces are associated with the wedges. The left and right boundaries L and R are both associated with configurational forces, however, by choosing the lengths L_{left} and L_{right} large enough, the stresses at these boundaries will be small and the associated configurational forces can be neglected. The intended position for the kink-band is centred in the notch, cf. Fig. 3. Figure 4 shows a close-up of the notch.

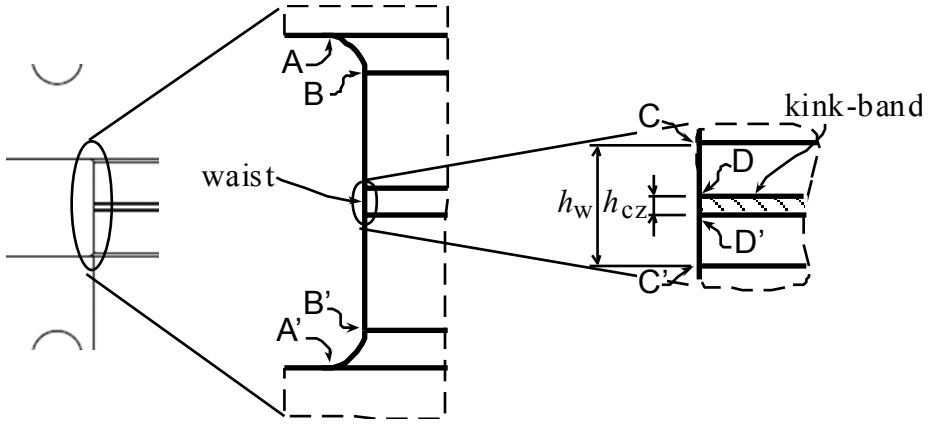

Figure 4. Close-up of notch with sub-areas, [4].

A configurational force P_{notch} is associated with the notch. Equation (3) gives

$$P_{\text{notch}} = \iint_{\text{AA'}} U\,\mathrm{d}y\mathrm{d}z = \underbrace{\iint_{\text{AA'}\notin\text{BB'}} U\,\mathrm{d}y\mathrm{d}z}_{P_{\text{r}}} + \underbrace{\iint_{\text{BB'}\notin\text{CC'}} U\,\mathrm{d}y\mathrm{d}z}_{P_{\text{b}}} + \underbrace{\iint_{\text{CC'}} U\,\mathrm{d}y\mathrm{d}z}_{P_{\text{w}}} \tag{6}$$

where the first integral results from choosing S in Eq. (3) as a closed surface closely adhering and enclosing the notch in the x-y-plane; the part of the surface with normal in the $\pm x_3$-direction can be chosen planar – as explained above, they do not contribute to P_{notch}. The second equality follows from a straight-forward split of the integral to a sum of parts from the different sub-areas identified in Fig.

Excerpt from ISBN 978-3-00-053387-7

4. The configurational forces P_r and P_b are evaluated from the experiments by utilizing our knowledge of the elastic properties of the material and measurements of the strain field close to the boundary using a Digital Image Correlation (DIC) system. The third configurational force of the notch P_w corresponds to the waist, cf. Fig. 4. By equilibrium of the configurational forces, P_w is written

$$P_w = P_{load} - P_r - P_b \tag{7}$$

where P_{load} is given by Eq. (2) as $F(\theta_1+\theta_2)$, cf. Fig. 3. A cohesive law is now associated with the waist. Equation (4) gives the corresponding configurational force

$$P_w\left(w_w\right) = b\int_0^{w_w} \sigma\left(\tilde{w}_w\right)\mathrm{d}\tilde{w}_w \tag{8}$$

where w_w is the compression of the waist. Setting Eqs. (7) and (8) equal, $\sigma(w_w)$ follows after differentiation. The cohesive law associated with the kink-band with measured height $h_{cz} \approx 200$ μm results after assuming a uniaxial state of stress at the boundary of the waist. Thus, with w_e denoting the compression of the waist outside the kink-band and E^* denoting the measured elastic stiffness of the waist,

$$w_e = \frac{\sigma\left(h_w - h_{cz}\right)}{E^*}. \tag{9}$$

The cohesive law is finally given by $\sigma(w) = \sigma(w_w\text{-}w_e)$. Figure 5 shows the results from one of the experiments reported in [4].

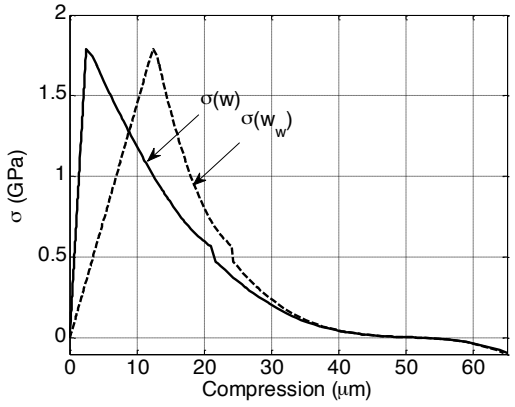

Figure 5. Measured cohesive law for waist $\sigma(w_w)$ (dotted curve) and for the kink-band $\sigma(w)$ (solid curve), [4].

It is noted that the fracture energy is about 25 kN/m, the maximum compressive stress is about 1.5 GPa and the compression at failure is about 50 μm. It should be noted that these data are associated with the formation of a kink-band in a less constrained state than in a cross-ply. With stiff plies outside the ply that forms the kink-band, the fibres will probably kink out more in the plane of the ply. For a detailed description of the experiments, the reader is referred to [4].

The present design succeeded in forming the kink-band in the intended position without introducing initial imperfections. A major challenge with the set-up is the measurement of the fields in the notch. The DIC-system is not ideally suited to measure strains close to an edge. Another challenge is to achieve a stable formation of the kink-band. A redesigned specimen has now been tested that provides better stability. The data remains to be evaluated.

Excerpt from ISBN 978-3-00-053387-7

5. Concluding remarks

Measurement of material data is always based on a more or less explicitly stated theory. The critical point in the present class of methods is the ability to associate a strain energy density U with the inelastic properties of the actual fracture process. At first sight, this might seem unfeasible. However, the difference between an inelastic and an elastic material is not observable from its stress-strain behaviour before unloading takes place. In non-linear fracture mechanics, the notion pseudopotential has been coined to distinguish between the potential of an elastic material and the (pseudo-)potential used in the analysis of the material cf. e.g. [11].

The two experimental set-ups presented here benefits from a relatively straight-forward identification of the material represented by the cohesive zone. With adhesive layers, the thickness of the layer constitute a well-defined definition of the height of the cohesive zone; with kink-band formation does the height of the kink-band provides a similar definition. Kink-band formation do, however, often show an increase in height with further loading. Thus, the height of the kink-band may increase and this should be considered in the development of a cohesive model of the phenomena. An example of a more challenging problem is the measurement of cohesive properties for delamination of a composite, cf. e.g. [12]. Here, it might be alluring to choose the resin rich material between the plies to be represented by the cohesive zone. However, this will often exclude parts of the material volume where the fracture process is active from the cohesive zone. Properly evaluated, this would lead to a too small fracture energy.

The methodology presented here have been extended to other load cases and to some extent to other problem areas. The results, i.e. the cohesive laws, are readily useable with some commercial FE-codes that provide cohesive finite elements. With these, strength analysis is reduced to a non-linear stress analysis.

It should be noted that both presented methods presented here are based on the application of transversal forces on test specimens. An alternative class of techniques where the load is applied by bending moments are developed by Sørensen and co-workers, cf. e.g. [13].

References

[1] J.D. Eshelby. The force on an elastic singularity. *Philosophical Transactions of the Royal Society of London. Series A*. 244:87-112, 1951.

[2] G.A. Maugin. Sixty years of configurational mechanics (1950–2010). *Mechanics Research Communications*, 50:39-49, 2013.

[3] U. Stigh, A. Biel, T. Walander. Shear Strength of Adhesive Layers - Models and Experiments. *Engineering Fracture Mechanics*. 129:67-76, 2014.

[4] D. Svensson D, K.S. Alfredsson, U. Stigh, N. Jansson. Measurement of cohesive law for kink-band formation in unidirectional composite. *Engineering Fracture Mechanics*. 151:1-10, 2016.

[5] S.P. Timoshenko, J.N. Goodier. *Theory of elasticity*. McGraw-Hill Kogakusha Ltd. 1970

[6] U. Stigh, T. Andersson. An experimental method to determine the complete stress–elongation relation for a structural adhesive layer loaded in peel. *Proceedings of the 2nd ESIS TC4 Conference on Polymers and Composites, Eds. J.G. Williams and A. Pavan, pp. 297-306. ESIS Publication 27, Elsevier, Amsterdam*, 2000.

[7] F. Nilsson. Large displacement aspects on fracture testing with double cantilever beam specimens. *International Journal of Fracture*. 139:305-311, 2006.

[8] T. Walander, A. Biel, U. Stigh. Temperature dependence of cohesive laws for an epoxy adhesive in Mode I and Mode II loading. *International Journal of Fracture*. 183:203-221, 2013.

[9] K.S. Alfredsson, U. Stigh. Stability of beam-like fracture mechanics specimens. *Engineering Fracture Mechanics*. 89:98-113, 2012.

Excerpt from ISBN 978-3-00-053387-7

[10] U. Stigh, K.S. Alfredsson, A. Biel. Measurement of cohesive laws and related problems. *Proceedings of the ASME International Mechanical Engineering Congress and Exposition IMECE2009, Lake Buena Vista, Florida, USA*, November 13-19, 2009.

[11] F. Nilsson. *Fracture mechanics—from theory to applications*. Department of Solid Mechanics, KTH, Stockholm, 2001.

[12] D. Svensson, K.S. Alfredsson, A. Biel, U. Stigh. Measurement of cohesive laws for interlaminar failure of CFRP. *Composites Science and Technology*. 100:53-62, 2014.

[13] R.K. Joki, F. Grytten, B. Hayman, B.F. Sørensen. Determination of a cohesive law for delamination modelling - Accounting for variation in crack opening and stress state across the test specimen width. *Composites Science and Technology*. 128:49-57, 2016.

Excerpt from ISBN 978-3-00-053387-7